IMPROVING HYPERSPECTRAL CLASSIFICATION BASED ONWAVELET DECOMPOSITION

O. Almog [a], M. Shoshany [a], V. Alchanatis [b], F. Qizel [a]

[a] Faculty of Civil and Environmental Engineering, Technion - Israel Institute of Technology, Haifa, Israel - almogo@tx.technion.ac.il

[b] Institute of Agricultural Engineering, ARO - The Volcani Center, Bet Dagan, Israel.

KEY WORDS: Remote Sensing, Hyperspectral, Classification, Calibration, Analysis, Data mining.

ABSTRACT:

Information extraction from Hyperspectral imagery is highly affected by difficulties in accounting for flux density variation and Bidirectional reflectance effects. Calculation of flux density requires digital description of the surface structure at the pixel level, which is frequently not available at the accuracy required (if exists). The result of these shortcomings in achieving accurate radiometric image calibration is reduced separability of surface types: limiting the performance of spectral classification schemes. In this study an alternative approach is presented: application of features of the spectral signature which mainly represent the shape of the spectral curve. This is achieved by applying features calculated based on Wavelet decomposition.

1. INTRODUCTION

Hyperspectral remote sensing involves image acquisition and analysis of spectral cubes, which are composed of tens and hundreds of narrow spectral bands. This process is used for extracting, identifying and classifying materials and environmental phenomena. The main assumption is that there are relations between the chemical, biological and physical properties of those materials and phenomena and the characteristics of their reflected radiation distribution. Those relations are the basis of remote sensing analysis (Landgrebe, 2002; Penn, 2002). The use of large number of narrow bands is supposed to increase classification accuracies. However, it seems that there are some obstacles in achieving these analysis improvements like: (1) various acquiring conditions such as: atmospheric conditions, illumination and relative sensor position; (2) various materials characteristics; (3) Lack of adequate information regarding the surface topography and micro-topography ; and (4) high dimensionality of information including noise added during the acquisition process.

In this study it is suggested to improve the spectral separation between surface objects under these conditions by applying features of the spectral signature which mainly represent the shape of the spectral curve. This is achieved by applying features calculated based on Wavelet decomposition.

Wavelet analysis is a space localized periodic analysis tool, which enables analysis of a signal in both time and frequency domains (Bruce et al, 2002; Kaewpijit et al, 2003; Kempeneers et al, 2005; Li, 2004). The reflectance signature is decomposed into different scale components; each scale component represents periodical behavior of the reflectance signature at that specific scale. The periodical behavior preserves the shape of the original reflectance signature. In an earlier study, Almog et al, (2006) presented that a selection of such scale components by itself may improve classification robustness. Here it is hypothesized that applying several relationships between wavelet coefficients and the original reflectance curve would be less affected by illumination intensity while preserving the unique features of each of the signatures. For applying those relationships, we transformed the reflectance signal into a new domain combined both radiometric and geometric information of the reflectance signal.

2. WAVELET TRANSFORME

Wavelet transform is a signal periodic analysis tool, which enables analyzing a signal in both time and frequency domains and consider it as a multi resolution process. The signal is analyzed by a mother wavelet function, which is translated relative to the signal in various extended scaling factors.

Wavelet transform output is a pyramidal form of coefficients; each of them describes the correlation between the mother wavelet function and a specific signal segment. The size and location are then derived from a corresponding scale and translation factors. Scaling process is achieved by stretching the mother wavelet among its spectral axis. Each of this stretching procedure reduces the mother wavelet frequency, and hence reduces the number of translations among the signal as well.

Initially at level 1, the mother wavelet scale is set to 1 and translated relative to the signal, such that each translation produces a correlation coefficient. All the coefficients calculated in the first step represent high frequencies hidden among the signal and called Detailed Coefficients at level 1. In the following step the mother wavelet is stretched, usually by a power of two, the level is ascended and the translation process relative to the signal is repeated. Figure 1 describes different mother wavelet scales. (1a) scale = 1, the mother wavelet is detailed and enables analysis of high frequencies along the signal. (1b) scale = 2, the mother wavelet is less detailed hence it enables analysis of lower frequencies along the signal. The number of points that define the mother wavelet at scale = 2 is halved compared to the number of points at scale = 1, hence, the number of translation is halved accordingly. Finally the coefficient pyramid consists of the maximum number of coefficients at first level, depending on chosen mother wavelet. Assuming scaling factor of 2, each ascending level consists of half the number of coefficients of the level above.

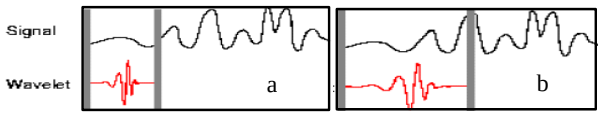

Figure 1. Correlation between mother wavelet to a specific signal segment (Matlab© documentation).

The wavelet mathematical description is given by:

$$C_x^{\psi}(\tau, s) = \frac{1}{\sqrt{|s|}} \sum_{t=0}^{T-1} x(t) \cdot \psi\left(\frac{t-\tau}{s}\right) \qquad (1)$$

Where: Cψ,x(τ,s) the correlation coefficient; τ is the translation location; s is the scaling factor for the specific iteration; x(t) is a signal in time domain with discretized length t and ψ is the wavelet mother function.

3. METHODOLOGY

3.1 Incident angle effects reduction

In this work we first assessed the reduction of the effects from differences in illumination angles by using wavelet first level detailed coefficients, extracted from the above described hyperspectral cubes data. In order to evaluate the efficiency of such reduction we calculated a normalized difference value between two curves representing two differential hyperspectral signatures of the same material acquired under different sun incident angles. For each band we calculated the differences between the intensity values divided by the difference between maximum and minimum values among both curves. The result of this calculation for each band was named Normalized Band Difference Index (NBDI) and is described as:

$$NBDI_i = \frac{hr_i - lr_i}{hr - lr} \qquad (2)$$

where hr_i is the highest signals value in the i^{th} band, lr_i is the lowest signals value in i^{th} band, *hr* is the absolute highest value among the signal, and *lr* is the absolute lowest value among the signal.

After calculating NBDI index for each band, we calculated the area below the NBDI graph to normalize the total amount of difference between two spectral signatures. This process was repeated for both spectral reflectance signatures and wavelet first coefficients. For the comparison of the dissimilarities we examined the area below each NBDI graph: the lower the area is, the higher the similarity. Fig. 2 illustrates vegetation spectral reflectance signature of one pixel, acquired under two different incident angles; a) spectral reflectance intensity; b) wavelet first detailed coefficients; c) normalized ratio at each band. The simulative incident angles were 0 and 45 degrees. We can observe that the dissimilarity in reflectance intensity values is greater in comparison to the dissimilarity in wavelet coefficients.

The areas under the NBDI curves shown in Fig. 2 which represent the relative dissimilarities in both spectral reflectance signatures and wavelet first coefficients, are 310 and 30 respectively. The results show that the relative dissimilarities occurred in the spectral reflectance signatures was reduced by a factor of 10 when using the wavelet first coefficients. In previous work [XX] we showed that by using wavelet first coefficients, the total dissimilarity is approximately five times lower than the one among the reflectance intensity signature. We assume that this difference occurred due to additional factors affecting the spectral reflectance signature such as atmospheric behavior, backscattering and more.

Different illumination conditions affect spectral reflectance intensity, but yet maintain the signature's geometric shape. Using wavelet transform, this shape is analyzed with relatively low influence by the intensity component, thus potentially reducing the illumination reflectance intensity effects.

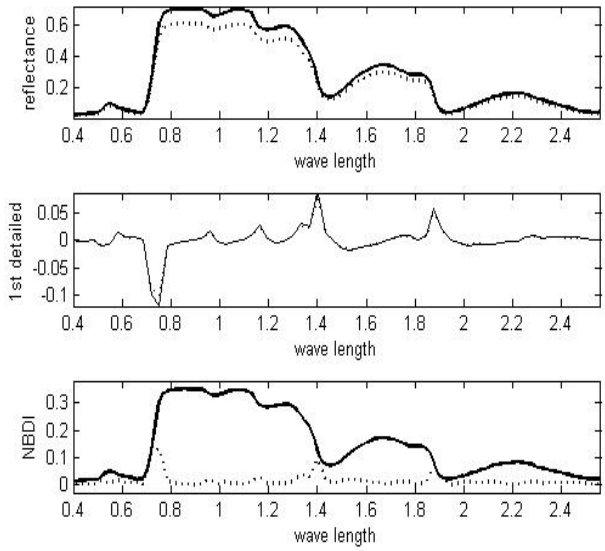

Figure 2. Two types of vegetation curves; a) spectral signature; b) wavelet first detailed coefficients; c) the NBDI curves.

3.2 Relations between wavelet coefficients and reflectance

Empirical assessment of material classification based on full wavelet coefficients had yielded moderate and low accuracies very similar to those obtained by classifying based on the spectral reflectance data itself. Thus we propose a new approach of using features that are based on ratios between reflectance intensity values and wavelet coefficients.

4. EXPERIMENTAL SETUP

The experimental setup included simulative and field data. The simulative data represented only illumination angle effects.

Some vegetation hyperspectral signatures were taken from known spectral libraries such as: USGS / JPL libraries. For simulating change in illumination angles we assumed that the library signatures were taken with a spectro-radiometer in ideal conditions in order to ensure analogue zero degrees incident angle. Radiation beam flux density, which hit an object, is depended mainly on incident angle; the lower the incident angle is, the higher the flux density. In order to simulate the incident angle effect we calculated reflectance intensity for each incident angle θ, thus simulating the intensity decrease via the cosine angle, which can be written as:

$$R_\theta = R_0 \cdot \cos\theta \qquad (3)$$

Where R_θ is the relative reflectance intensity achieved under incident angleθ, and R_0 is the reflectance intensity achieved under zero incident angle.

In this experiment we have chosen seven different vegetation types: (1) black-brush; (2) fir tree; (3) maple leaves; (4) pinon pine; (5) Russian olive; (6) sage brush and (7) walnut leaf.

For each vegetation type we randomly simulated about 700 simulative spectral curves affected by incidence angles (using equation 3) between 0 and 55 degrees. Eventually, there were 5,000 of such hyperspectral signatures taken under various incident angles divided into seven sets. The next stage was to choose some training and testing population. Classification was then performed once on the simulative spectral data itself and once on the data representing the parametric relations between the wavelet coefficients and the reflectance data.

The classification process was based on Linear Discriminate Analysis (LDA); the maximum-likelihood criterion was used to assign an inquired signature to its class. We used supervised classification, where it is possible to examine the quality of assigning a signature to its true class. The classifier was first trained using a training set of pixels with their known corresponding classes. Then, classification performance was evaluated using a test set, consisting of pixels that were not used for the training process. The success of classification assignments of the test set were summarized for assessing the classification success rates.

5. RESULTS

Applying the supervised classification method described above, we used 1% of the total 5,000 simulative hyperspectral signatures as training set. In order to avoid a bias in the training or test procedure, we repeated 5 times the classification process, where the training sets were chosen randomly. The following results represent the average rate of classification success:

The average success rates based on spectral reflectance signature were 76%, 77% and 72% respectively.

The success rates based on relations between reflectance and wavelet coefficients were 100% for consistently.

Table 1 describes the confusion matrix using the spectral reflectance values. The number of pixels in each class is depicted in the second line of the table. The total number of misclassified pixels was 1345, which corresponds to a 27% error rate (and hence 73% success rates). It can be seen that for three groups the success rates are 100%. This is due to well separated signatures between the vegetation types.

The training set size was again 1% of the total sample size. The results show a 100% of success rate. Using those relations reduced the misclassified pixels from 1,345 signatures in reflectance domain to zero. These results indicate that using the proposed relations enabled us to isolate the effect of incident angle out of the total acquisition process effects. The significant improvement of the success rate, up to 100%, illustrates the strong correlation between geometric and radiometric characteristics of the signatures. The former is embodied through wavelet coefficients, while the later through intensity values.

Table 1 : confusion matrix
for classification based on spectral reflectance

Number of pixels in each class	629	647	615	608	644	615	1192	
Misclassified pixels	7	6	5	4	3	2	1	
559	0	0	0	559	0	0	633	1
203	0	0	0	123	0	412	80	2
0	0	0	0	0	644	0	0	3
389	0	0	0	219	0	257	132	4
194	194	0	421	0	0	0	0	5
0	0	647	0	0	0	0	0	6
0	629	0	0	0	0	0	0	7
Group success rates	100	100	68	36	100	67	53.1	

Table 2 : confusion matrix for classification based
on relation between reflectance and wavelet coefficients

Number of pixels in each class	629	647	615	608	644	615	1192	
Misclassified pixels	7	6	5	4	3	2	1	
0	0	0	0	0	0	0	1192	1
0	0	0	0	0	0	615	0	2
0	0	0	0	0	644	0	0	3
0	0	0	0	608	0	0	0	4
0	0	0	615	0	0	0	0	5
0	0	647	0	0	0	0	0	6
0	629	0	0	0	0	0	0	7
Group success rates	100	100	100	100	100	100	100	

Table 2 describes the confusion matrix using the relations between reflectance and wavelet coefficients.

Note that the classified entities are all associated with different species of vegetation, which are characterized by similar spectral reflectance signature.

6. CONCLUSION

Remote sensing based on spectral reflectance intensity is sensitive to acquisition process effects. These effects remain although some calibration processes are carried out. This is due to limitations in assessing several of the external parameters that affect the intensity value in hyper-cubes while being acquired. However, the shape of these signatures is much less influenced by those conditions. Linking both radiometry and shape parameters, which are derived from an acquired hyper-cube, leads to a reduction in dissimilarities that exist in the same materials' signature. We introduced that linkage by using the RG ratio, where we shown that it is possible to improve classification success rates, and hence a
better understanding of the acquisition conditions that affect the hyperspectral reflectance intensity analysis.

REFERENCES

A. Grapes, 1995. "An introduction to wavelet". Computational Science and Engineering, IEEE Volume 2, Issue 2, Summer 1995 Page(s):50 – 61.

Bruce L., Koger C.H., Li j., 2002. Dimensionality Reduction of Hyperspectral Data Using Discrete Wavelet Transform Feature Extraction. IEEE TRANSACTION ON GEOSCIENCE AND REMOTE SENSING, VOL. 40, NO10, OCTOBER 2002.

Cierniewski J., 1987. A Model for Soil in the Visible and Near-Infrared Range. Remote Sensing of Environment, 27, 135-142.

Gonzales R.C, Woods R.E., 1993. Digital Image Processing. Addison-Wesley Publishing Company.

Healey G., Slater D., 1999. Models and Methods for Automated Material Identification in Hyperspectral Imagery Acquired Under Unknown Illumination and Atmospheric Conditions. IEEE Transaction on Geoscience and Remote Sensing, Vol. 37, No. 6, November 1999.

Kaewpijit S., Le Moigne J., El-Ghazawi T., 2003. Automatic Reduction of Hyperspectral Imagery Using Wavelet Spectral Analysis. IEEE Transactions on Geoscience and Remote Sensing, Vol. 41, No. 4, April 2003.

Kempeneers P., De Backer S., Debruyn W., Coppin P., Scheunders P., 2005. Generic Wavelet-Based Hyperspectral Classification Applied to Vegetation Stress Detection. IEEE TRANSACTIONS ON GEOSCIENCE AND REMOTE SENSING, VOL. 43, NO. 3, MARCH 2005.

Landgrebe D., 2002. Hyperspectral Image Data Analysis as a High Dimensional Signal Processing Problem. Special Issues of the IEEE Signal Processing Magazine, Vol. 19 No.1 pp. 17-28, January 2002.

Miller H.J., Han J., 2001. Geographic Data Mining and Knowledge Discovery: an overview. Geographic Data Mining and Knowledge Discovery pp. 3-32. Taylor & Francis, London, UK.

Penn B.S., 2002. Using Simulated Annealing to Obtain Optimal Linear End-Member Mixture of Hyperspectral Data. Computers & Geosciences 28 (2002) 809-817.

Shoshany M., 1991, The Equifinality of Bidirectional Reflectance Distribution Functions of Various Microstructures. Int J. Remote Sensing, 1991, Vol. 12 No. 11, 2267-2281.

Shoshany M., 1993. Roughness-Reflectance Realationship of Bare Desert Terrain: An Empirical Study. Remote Sens. Envbiron. 45:15-27 (1993).

Thenkabail, P., Enclon€a, E., Ashton, M., Van der Meer, B., 2004, Accuracy Assessment of Hyperspectral Waveband Performance for Vegetation Analysis Applications. Remote Sensing of Environment. Pages??

Tomiya M., Ageishi a., 2003. Registration of Remote Sensing Image Data Based on Wavelet Transform ISPRS Archives, Vol. XXXIV, Part 3/W8, Munich, 17-19. Sept. 2003.